A regenerable biosensing platform for bacterial toxins

E. Eduardo Antunez,[a,b,±] *Clare S. Mahon,*[c,±] *Ziqiu Tong,*[a] *Nicolas H. Voelcker,*[a,b,*] *and Markus Müllner*[d,e,*]

[a] Monash Institute of Pharmaceutical Sciences, Monash University, Parkville, Victoria 3052, Australia; [b] Melbourne Centre for Nanofabrication, Victorian Node of the Australian National Fabrication Facility, Clayton, Victoria 3168, Australia; [c] Department of Chemistry, Durham University, Durham, DH1 3LE, UK; [d] Key Centre for Polymers and Colloids, School of Chemistry, The University of Sydney, Sydney 2006, New South Wales, Australia; [e] The University of Sydney Nano Institute (Sydney Nano), Sydney 2006, New South Wales, Australia.

[±] authors contributed equally;

KEYWORDS: porous silicon, thermoresponsive, infectious disease, polymers, *E. coli*

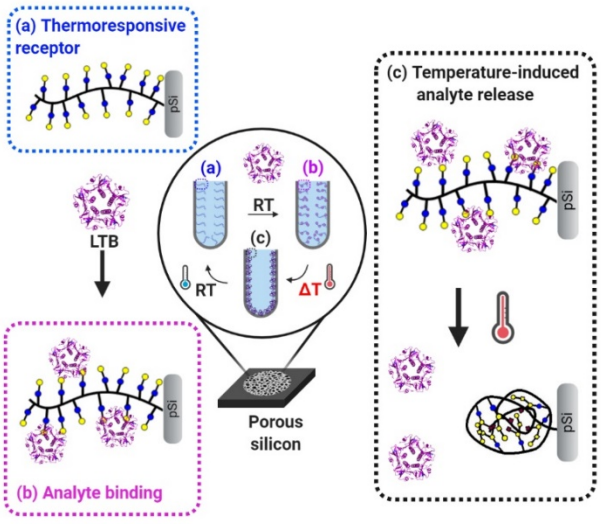

ABSTRACT
Waterborne diarrheal diseases such as travelers' diarrhea and cholera remain a threat to public health in many countries. Rapid diagnosis of an infectious disease is critical in preventing the escalation of a disease outbreak into an epidemic. Many of the diagnostic tools for infectious diseases employed today are time-consuming and require specialized laboratory settings and trained personnel. There is hence a pressing need for fit-for-purpose point-of-care (POC) diagnostic tools with emphasis in sensitivity, specificity, portability, and low cost. We report work towards thermally reversible biosensors for detection of the carbohydrate-binding domain of the *E. coli* heat-labile enterotoxin (LTB), a toxin produced by enterotoxigenic *E. coli* strains, which causes travelers' diarrhea. The biosensing platform is a hybrid of two materials, combining the optical properties of porous silicon (pSi) interferometric transducers, and a thermoresponsive multivalent glycopolymer to enable recognition of LTB. Analytical performance of our biosensors allow us to detect, using a label-free format, sub-micromolar concentrations of LTB in solution as low as 0.135 μM. Furthermore, our platform shows a temperature-mediated 'catch-and-release' behavior, an exciting feature with the potential for selective protein capture, multiple readouts, and regeneration of the sensor over consecutive cycles of use.

INTRODUCTION
Waterborne disease presents a challenge to public health systems on a global scale. Approximately 1.7 bn people are estimated to use a source of drinking water that has been subject to fecal contamination,[1] placing them at substantial risk of contracting bacterial gastroenteritis. In 2016, diarrheal disease caused 1.6 m deaths – primarily in the developing world, with over 25% of those deaths occurring in children under the age of five.[2] Two bacterial pathogens that are responsible for a significant proportion of these cases are *V. cholerae*, the causative agent of cholera, and enterotoxigenic strains of *E. coli* (ETEC), which cause the more prevalent, if less severe, travelers' diarrhea.[3] These pathogens both colonize the human intestine and cause disease through the production of protein toxins, the cholera toxin (CT) and the *E. coli* heat-labile enterotoxin (LT), respectively. These toxins are structurally and functionally related, belonging to the AB_5 family of toxins, with 80% sequence homology.[4] Each consists of a toxic A subunit and a pentamer of identical B-subunits (termed CTB/LTB), which each contain a recognition site for the GM1 ganglioside, a complex carbohydrate displayed on mammalian cellular surfaces and exploited by the toxins to gain cellular entry. Recognition of the pentasaccharide head group of the GM1 ganglioside, the GM1 oligosaccharide (GM1os), by CTB has been demonstrated to be of remarkably high affinity, with K_d ~40 nM.[5]

Given the prime importance of this cellular recognition to the virulence of these bacteria, species that can modulate or inhibit the interaction are attractive candidates for the design of new therapeutics and diagnostics. A number of multivalent receptors and inhibitors for CTB/LTB have been produced by incorporating multiple copies of the GM1os recognition motif onto a macromolecular scaffold,[6] such as a dendrimer,[7] synthetic polymer, or engineered protein.[8] Multivalent effects can also greatly enhance the recognition capabilities of simplified carbohydrate motifs, the use of which would be beneficial in terms of decreasing the costs and time associated with receptor generation. For example, CTB binds to methyl-β-D-galactopyranoside, a structural analogue of the terminal galactose residue of GM1os, with K_d ~15 mM,[5] a decrease of six orders of magnitude compared with the pentasaccharide motif. Remarkable improvements in recognition have been achieved by appending multiple copies of these simplified recognition motifs onto macromolecular scaffolds, with 10^6-fold enhancements in inhibitory potency observed for decavalent D-galactose receptors,[9] bringing inhibitory potencies into the nanomolar range. Likewise, polymers displaying multiple copies of galactose recognition motifs have been demonstrated to complex with LTB with K_d values in the low micromolar range.[10]

Glycan-based biosensing is an attractive approach to the development of diagnostic devices for a wide range of diseases, as many pathogens produce lectins which interact with cell-surface carbohydrates.[6] Carbohydrate-decorated conductive polymers, for example, have been used as sensors for label-free detection of bacteria through surface lectin recognition.[11] Glycan microarrays[12] based on gold nanoparticles or surfaces have been used to detect lectins including RCA_{120}, a model for the ricin toxin.[13,14] The incorporation of oligosaccharides that are displayed on cellular surfaces into biosensors can allow for the detection of disease-associated lectins. Immobilization of 3'-sialyllactose onto gold surfaces has enabled the preparation of impedance-based biosensors for influenza haemagglutinins, for example.[15] Similarly,

analogues of the mammalian glycolipid Gb3 have been used to detect the Shiga toxin (Stx1), produced by the acutely virulent *E. coli* O157:H7 in ELISA assays.[16] Here, we have used thermoresponsive polymers displaying multiple copies of GM1os, and a simplified lactose recognition motif, as multivalent receptors for LTB, enabling the production of responsive hybrid biosensors when integrated with inorganic porous silicon (pSi) optical transducers.

Thermoresponsive polymers such as poly(*N*-isopropylacrylamide) (poly(NIPAm)) can be used to tune the recognition of glycoconjugates by lectins, with reports of materials displaying either decreased or enhanced recognition abilities above and below the LCST. Differences in behavior can arise as a consequence of system design, resulting in differences in ligand accessibility associated with the phase transition. Gibson and coworkers[17] have used surface-appended poly(NIPAm) to control the presentation of carbohydrates on gold nanoparticles. Below the LCST of the polymer, its steric bulk prevents interaction with lectins, with hydrophobic collapse exposing carbohydrate units on the surface of the nanoparticles. Above the LSCT of a glycopolymer, it could be argued that carbohydrate moieties are rendered inaccessible by coil to globule collapse, but it could also be expected that under these conditions the surface presentation of hydrophilic sugar units would be preferred. Behavior consistent with both hypotheses has been observed. Glucose-functionalized poly(NIPAm)s have been shown to promote aggregation of *E. coli* bearing the FimH lectin below their LSCT, with increase in temperature above the LCST leading to dispersal of aggregates.[18] Conversely, mannose functionalized poly(NIPAm) microgels have been shown to display enhanced affinities for the complementary lectin Con A and FimH bearing *E. coli.*[19] Recent work by Schmidt and coworkers has highlighted the variation in behavior that may be observed even with the same thermoresponsive system.[20] The interactions of mannose-functionalized poly(NIPAm)s with Con A, and *E. coli* displaying FimH, were studied via quantitative adhesion inhibition assays. While the inhibition of Con A was reduced above the cloud point of the polymers, the inverse behavior was observed for *E. coli* inhibition. The avidity of the thermoresponsive glycopolymer system used in this study for CTB has been demonstrated to decrease above the LCST of the polymer through isothermal titration calorimetry experiments.[21]

Porous silicon (pSi) is a versatile nanostructured material comprising air-filled pores with dimensions less than 150 nm in a silicon matrix.[22] pSi presents tunable photonic and morphological properties, and its fabrication process is relatively simple and cost-effective. In particular, the simplest geometry, the single-layer pSi interferometer, has gained sustained research interest due to its optical transducing features (i.e., Fabry–Pérot interference),[23] large internal surface area (up to 800 $m^2 g^{-1}$) producing surfaces able to accommodate a variety of (bio)receptors and monitor (bio)molecular interactions occurring within its pores,[24] and presenting a highly reactive surface for further functionalization using a variety of well-established chemical derivatization strategies.[25]

Single-layer pSi interferometers and more complex photonic structures, (i.e., double-layers, Bragg stacks, microcavities, rugates) can serve as a host matrix for the integration of a variety of materials such as fluorescent molecules,[26] quantum dots (QDs),[27] carbon dots (C-dots),[28] metallic nanoparticles,[29] and polymers.[30–32] On this latter point, pSi-based hybrid composites integrating thermoresponsive polymeric materials have attracted significant attention due to the synergy between the unique photonic and morphological properties of pSi and the thermally-driven response of these polymers, leading to the preparation of pSi-polymer platforms that could exhibit superior sensing performance in comparison to their individual components. These hybrid sensors demonstrate promise in a number of applications as diverse as drug delivery, actuation and biosensing.[33–38] Microfluidic devices are increasingly incorporated to facilitate biosensor portability and automation, reduced sample and reagent consumption and allow for real-time detection.

To the best of our knowledge, only one study by Kilian *et al.* has reported using pSi-based transducers for the detection of bacterially produced toxic proteins related to infectious diseases such as travelers' diarrhea or cholera.[39] They reported on CTB detection using a biomimetic interface method where a rugate photonic structure was functionalized with hybrid lipid bilayer membranes containing the GM1os receptor. This system enabled the detection of sub-micromolar concentrations of CTB (1 nM). Detection required, however, an extended incubation time of 4 h to produce reliable responses.

We present a new 'catch-and-release' biosensor by combining the functionality of a multivalent and stimulus-responsive polymer receptor with the label-free transduction capabilities of pSi interferometers. Our simple polymeric receptor contains multiple lactose/GM1os recognition motifs that allow for a selective 'catch' of the target analyte, including sub-micromolar concentrations of LTB, and the triggered 'release' of the protein after detection. The thermoresponsive nature of the polymeric receptor allows this biosensor to be reused for subsequent detection cycles, presenting a regenerable detection platform.

EXERIMENTAL DETAILS

Materials

The following reagents and chemicals: absolute ethanol (EtOH, 99.9%), anhydrous toluene (99.8%), diethyl ether (Et_2O), sodium chloride (NaCl, 99.5%), sodium hydroxide (NaOH, 98%), hydrochloric acid (HCl, 37%), 2-(*N*-morpholino)-ethanesulfonic acid (MES buffer, 99%), *N*-(3-dimethylaminopropyl)-*N*′-ethylcarbodiimide hydrochloride (EDC), *N*-hydroxysuccinimide (NHS, 98%), (3-aminopropyl)trimethoxysilane (APTMS, 97%), dimethyl sulfoxide (DMSO), streptavidin from *Streptomyces avidinii* (SA), succinic anhydride and concanavalin A (Con A) were purchased from Sigma Aldrich (Australia) and used as supplied unless otherwise indicated. *N*-Isopropylacrylamide (NIPAm) was purchased from Sigma Aldrich and recrystallized from hexane. α,α′-Azoisobutyronitrile (AIBN) was purchased from Sigma Aldrich and recrystallized from ethanol prior to use. *tert*-Butyl 2-methacryloylhydrazine-1-carboxylate (**M1**), and GM1os were prepared as described previously.[21] S-1-Dodecyl-S'-(α,α-dimethyl-α''-acetic acid) trithiocarbonate (DDMAT) was prepared according to a literature procedure.[40] Boron-doped (p^{++}-type) silicon wafers (100)-oriented and resistivity of 0.55 – 1 mΩ·cm, were purchased from Sil'tronix (France). Aqueous hydrofluoric acid (HF, 48%) was purchased from Honeywell (Chem-Supply Australia). Aqueous buffer and solutions were prepared using MilliQ (Merck Millipore, Australia), filtered using syringe filters (0.2 μm, polyethersulfone (PES) membrane, PALL), and pH-adjusted with NaOH (1 M) and HCl (1 M) aqueous solutions.

Synthesis of P1

P1 was prepared using a similar strategy to that reported previously.[21] DDMAT (10 mg, 2.7 x 10^{-5} mol, 1.0 eq.), AIBN (1.0 mg, 5.5 x 10^{-6} mol, 0.2 eq.), NIPAm (0.496 g, 4.38 x 10^{-3} mol, 160 eq.) and **M1** (0.110 g, 5.5 x 10^{-4} mol, 20 eq.) were combined in DMSO (1.5 mL). The solution was sparged with N_2(g) for 15 min before the vessel was sealed under N_2(g) and placed in a preheated oil bath at 70 °C. After 17 h, the solution was flash frozen in $N_{2\,(l)}$ and exposed to air. The reaction mixture was diluted with DMSO and added dropwise to a large excess of ice-cold Et_2O, yielding a yellow solid which was redissolved in dioxane and precipitated again from Et_2O. **P1** was isolated by filtration as a yellow-white solid and dried under high vacuum (0.463 g). ^{1}H NMR: (500 MHz, $CDCl_3$): δ 0.88 (t, J = 6.8 Hz, ω-CH_3), 1.12 (br, NHCH(CH_3)$_2$), 1.45 (br, COOC(CH_3)$_3$, 1.5 – 2.4 (br, C*H*, CH_2, CH_3 (polymer backbone), 2.89 (br, N*H*), 3.99 (br, NHC*H*CH_3), 5.8 – 7.1 (br, N*H*NCOOC(CH_3)$_3$). Refer to Supporting Information S1 for further details.

Synthesis of P2

P2 was prepared using a similar strategy to that reported previously.[21] **P1** (100 mg, 9.26 x 10^{-6} mol) was dissolved in CH_2Cl_2 (3 mL). Trifluoroacetic acid (3 mL) was added, and the reaction mixture was left to stir at room temperature for 90 min. The solution was evaporated to dryness, yielding a yellow film, which was taken up in H_2O. The crude product was dialyzed against H_2O and lyophilized, yielding a yellow-white solid (84 mg, 94%). ^{1}H NMR: (400 MHz, D_2O): δ 1.08 (br, NHCH(CH_3)$_2$,), 1.2–1.6 (br, (CH_2, CH_3), polymer backbone), 1.93 (br, CH (polymer backbone), 3.83 (br, NHC*H*CH_3). Refer to Supporting Information S1 for further details.

Synthesis of thermoresponsive polymeric receptor P2-Lac

P2 (10 mg, 1.0 x 10^{-6} mol) was dissolved in 100 mM NH_4OAc pH 4.5 (1 mL). Lactose monohydrate (26 mg, 1.2 x 10^{-5} mol, 70 eq.) was added, and the reaction mixture was left to stir at room temperature overnight. The solution was dialyzed against H_2O and lyophilized to afford the title product as a yellow-white solid (12 mg, 84%). For ^{1}H NMR spectrum see Fig. S4.

Synthesis of thermoresponsive polymeric receptor P2-GM1os

P2 (8.0 mg, 8.2 x 10^{-7} mol) was dissolved in 100 mM NH_4OAc pH 4.5 (1.25 mL). GM1os (13 mg, 1.2 x 10^{-5} mol, 15 eq.) was added, and the reaction mixture was left to stir at room temperature overnight. The

solution was dialyzed against H_2O and lyophilized to afford the title product as a yellow-white solid (14 mg, 72%). For ^1H NMR spectrum see Fig. S5.

Expression of LTB

Cells from a glycerol stock of *Vibrio sp60* harboring plasmid pMMB68[41] were used to inoculate growth medium (100 mL, 25 g/L LB mix, 15 g/L NaCl, ampicillin 100 μg/mL). The culture was grown overnight at 30 °C with shaking at 200 rpm, then used to inoculate fresh growth medium (6 x 1 L, 25 g/L LB mix, 15 g/L NaCl, ampicillin 100 μg/mL). These cultures were incubated at 30 °C with shaking at 200 rpm until A_{600} reached 0.6, before protein expression was induced by addition of isopropyl □-D-1-thiogalactopyranoside to a concentration of 0.5 mM. Cultures were incubated (30 °C, 200 rpm) for a further 24 h, then cells were removed by centrifugation (7500 *g*, 15 min). The combined supernatant was treated with ammonium sulfate (550 g/L) and left to stir at 5 °C for 2 h. Crude protein was isolated by centrifugation (17000 *g*, 25 min) and redissolved in 100 mM NaH_2PO_4, pH 7.0, 500 mM NaCl (60 mL). Insoluble material was removed by centrifugation (5000 *g*, 10 min) before the solution was passed through a 0.22 μm nylon filter then loaded onto a lactose-sepharose 6B column and eluted with 300 mM lactose, 100 mM NaH_2PO_4, pH 7.0, 500 mM NaCl. LTB was dialyzed against phosphate buffered saline at pH 7.4 (PBS: 137 mM NaCl, 2.7 mM KCl, 10 mM Na_2HPO_4, 1.8 mM KH_2PO_4), freeze-dried and stored at -20 °C.

Fabrication of pSi interferometers and functionalization

pSi surfaces were fabricated by electrochemical dissolution of p^{++}-type crystalline silicon (Si) wafers using an electrolyte solution of hydrofluoric acid (HF, 48%) in absolute ethanol in a volumetric ratio of 1:1, respectively. Electrochemical anodization was performed using a Teflon cell by applying an electrical current (driven by a Keithley 2612 source meter unit) between the flat aluminum foil underneath the Si wafer and a platinum electrode. Briefly, the Si wafer was pre-treated by anodic etching at a current density of 50 mA cm^{-2} for 30 s to avoid the formation of a parasitic layer, which restricts the diffusion of the analytes into the pSi layer. The pSi sacrificial layer was then dissolved by exposure to NaOH solution (1 M) for 120 s, followed by rinsing with ultrapure water and dried under a flow of nitrogen gas. The pre-treated surfaces were etched to produce pSi interferometers by applying the current density and time values listed in Table 1. Next, the freshly etched pSi substrates were thermally oxidized at 600 °C for 1 h in air using a tubular furnace (Labec, Australia), followed by ozone oxidation at a flow rate of 5.0 g m^{-3} at 0.5 L min^{-1} oxygen for 30 min by use of a UV-1 UV-ozone cleaner (SAMCO Inc., Kioto, Japan). The substrates were then incubated with APTMS (57 mM) for 10 min at room temperature in anhydrous toluene to introduce amine groups onto the pSi surface. The surfaces were washed three times with anhydrous toluene, dried under a stream of nitrogen gas, and cured at 100 °C for 10 min to remove any trace of the solvent and to increase crosslinking density of the formed silane layer.[27]

Table 1. Etching conditions used to fabricate the pSi interferometers and resulting film parameters.

Surface No.	Current density (mA cm^{-2})	Etching time (s)	Pore diameter[a] (nm)	Thickness[a] (nm)	Porosity[b] (%)
1	5.8	633	13 – 25	2156	76
2	11.6	364	19 – 28	2200	78
3	28.3	175	24 – 37	2190	82
4	41.6	117	32 – 58	2280	84
5	50	100	37 – 70	2100	86
6	41.6	90	32 – 58	1650	84
7	41.6	175	32 – 58	3155	84

[a] As determined by SEM analysis. [b] As determined by a simulation program (SCOUT, obtained from W. Theiss Hard- and Software), which is based on the transfer matrix method; the best fit between the experimental and theoretical reflectivity spectrum was used to determine the porosity of the pSi films.

Preparation of pSi-polymer biosensor

The **pSi/P2-Lac** and **pSi/P2-GM1os** biosensors were prepared by covalent immobilization of the **P2-Lac** or **P2-GM1os** material onto the amino-functionalized pSi surfaces. The carboxylic acid end group of each polymeric receptor was activated by dissolving the polymer (7 mg mL^{-1}) in MES buffer (0.1 M, pH 4.5)

containing EDC (50 mM) and NHS (50 mM). The solution reacted for 30 min at room temperature. 20 µL of the solution was applied to each sensor and the surfaces were incubated at room temperature in a moist environment overnight. The pSi-polymer hybrid surfaces were several times thoroughly rinsed with ultrapure water and dried under a gentle flow of nitrogen gas.

Fabrication of microfluidic chip

A low volume flow-cell biosensor was fabricated in polydimethylsiloxane (PDMS) by photolithography and soft lithography.[42] Briefly, a chrome mask containing three parallel channels (1 x 5 mm^2; 1 x 7 mm^2; and 1 x 5 mm^2) were designed using Tanner L-Edit software and fabricated by direct write lithography (Intelligent Micropatterning SF100 XPRESS). A silicon wafer (3") was first cleaned with acetone, then isopropanol, and baked on a hot plate at 200 °C for 10 min for dehydration. SU-8 3050 (MicroChem) was spun at 1000 rpm using a spin coater, resulting in a layer of 100 µm thick SU-8 and baked at 95 °C for 45 min. The chrome mask was then aligned onto the silicon wafer coating with SU-8 and exposed to UV at 250 mJ cm^{-2} (EVG 6200 Mask Aligner). The UV-exposed silicon wafer was then baked for 1 min at 65 °C and 5 min at 95 °C. The silicon wafer was then transfer to a beaker containing SU-8 Developer (MicroChem) for gentle agitation for 5 min to remove the non-crosslinked SU-8. The silicon wafer containing SU-8 patterned feature was then incubated with trichloro(1H,1H,2H,2H-perfluorooctyl)silane (Sigma Aldrich) inside a vacuum desiccator overnight. PDMS (Dow Chemical) prepolymer and catalyst (10:1) were mixed thoroughly and poured onto the SU-8 patterned silicon wafer. The wafer was first degassed inside a desiccator and then transferred to an oven for 2 h at 80 °C. The cured PDMS was peeled off from the silicon wafer. The inlets and outlets of the microfluidic channels were created using a biopsy punch (1 mm in diameter). The final PDMS replica was cleaned with ethanol and then MilliQ water.

Optical biosensing

The experimental setup for the biosensing experiments is shown in Scheme 1. Briefly, white light from a tungsten lamp (HL-2000, Ocean Optics) was fed through one end of a fiber-optic reflection probe and focused through a collimating lens onto the surface of the pSi interferometer at normal incidence. The spotlight (1 mm in diameter) was then focused in the center of the sample's surface enclosed within one of the channels of the microfluidic chip adhered onto the pSi surface. The microfluidic chip serves as a low volume flow-cell enabling pSi to be used as a real-time interferometric biosensor. Light reflected from the pSi surface was collected through the same optics, and the distal end of the bifurcated optical reflection probe was coupled to a CCD spectrophotometer (HR2000+ES, Ocean Optics). Information about the conformation of the polymeric receptors, and the presence or absence of analyte within the nanopores, can be determined by monitoring changes in the reflectivity spectrum of the pSi-polymer hybrid surface. The reflectivity spectrum consists of a series of interference fringes that result from the Fabry–Pérot interference at the top and bottom boundaries of the pSi layer. The position of the fringe maxima is given by the following equation:

$$m\lambda = 2nL \quad (1)$$

where m is the spectral order, n is the average refractive index of the film, L is the physical thickness of the layer, and λ is the wavelength of the incident light. The factor of 2 derives from the 90° backscatter configuration of the illumination source and detector. The term $2nL$ is referred to as effective optical thickness (EOT) in this work. A change either in n or L produces a shift in the reflectivity spectrum and a change in EOT, respectively. The magnitude of EOT is extracted from the reflectivity spectrum by applying a fast Fourier transform (FFT) yielding to a single peak whose position and intensity along the x-axis correlate with the refractive index of the pSi layer. For FFT analysis, reflectivity spectra were recorded in the wavelength range of 500 to 1000 nm, with a spectral acquisition time of 100 µs. Typically, 10 spectral scans (1 s integration time) were averaged using SpectraView software (Ocean Optics). FFT values of the recorded reflectivity spectra were processed using IGOR PRO from Wavemetrics Inc. (www.wavemetrics.com) to obtain the EOT values as a function of time throughout the experiment, as detailed in a previously published procedure.[36]

In a typical biosensing experiment, a baseline was recorded in buffer (PBS, pH 7.4) followed by the introduction of LTB at different concentrations using a syringe pump. A flow rate of 5 µL min^{-1} was kept constant throughout the experiment (i.e., baseline establishment, exposure to LTB and rinsing steps) unless

otherwise specified. Exposure of the biosensor to LTB for complexation was performed for at least 30 min before the rinsing procedure. Afterward, the unbound analyte was removed by rinsing with buffer. Reflectivity spectra were collected and processed using FFT analysis, as already described. Data are presented as EOT(%):

$$EOT(\%) = \left(\frac{EOT - EOT_0}{EOT_0}\right) * 100 \quad (2)$$

where EOT refers to the averaged EOT magnitude obtained from the readout of the biosensor, and EOT_0 is the averaged EOT value obtained during baseline establishment at the beginning of the experiment. Biosensing experiments were performed at room temperature unless otherwise specified. Thermally-triggered 'catch-and-release' behavior of the biosensors was investigated upon consecutive heating-cooling cycles. An external water Peltier system (PCB 1500, PerkinElmer) interconnected to a purpose-built thermostable holder was used to control the heating and cooling cycles (5 °C min^{-1}) during the experiments. A flow rate of 10 µL min^{-1} was applied to mitigate the risk of evaporation of the carrier buffer solution within the channel of our microfluidic flow-cell when the biosensor was subjected to consecutive heating cycling (50 °C). This flow rate was kept constant throughout the temperature-controlled experiments.

Other characterization techniques

The nuclear magnetic resonance (NMR) spectra were recorded using a JEOL-ECS 400 or a Bruker Avance 400 spectrometer, with ^1H at 400 MHz, using the residual solvent signal as an internal standard. Gel permeation chromatography (GPC) analysis was conducted using a Shimadzu Prominence instrument equipped with a refractive index detector and a pair of Phenogel columns (Phenomenex, 300 x 7.8 mm^2; 5 µm 104 Å and 500 Å) in series, at 50 °C with dimethylacetamide (DMAc) containing LiBr (0.03%, w/v) as the eluent. Near monodisperse poly(methyl methacrylate) (PMMA) standards were used for calibration. Differential scanning calorimetry (DSC) experiments were performed at a polymer concentration of 2.0 mg mL^{-1} in PBS using a Microcal VP-DSC. The reference cell was filled with degassed PBS and the sample cell with polymer solutions. Solutions were held at 5 °C for 15 min, then heated to 80 °C at a rate of 90 °C h^{-1} before the cycle was repeated 10-20 times. Baseline scans of PBS were subtracted from scans of polymer solutions prior to data analysis. Scanning electron microscopy (SEM) was conducted on FEI Nova NanoSEM 430 using an accelerating voltage of 10 kV. As-fabricated pSi and polymer-modified pSi surfaces were cut into small sections before SEM analysis. Fourier transform infrared (FTIR) spectra were recorded using a Nicolet 6700 (Thermo Scientific) instrument in the attenuated total reflection (ATR) mode over the range of 650 to 4000 cm^{-1}, at a resolution of 4 cm^{-1} and averaging 64 scans. Background spectra were recorded using air and data processed using OMNIC software (Thermo Scientific). Static water contact angle (WCA) images were collected using a custom-built goniometer with a Panasonic CCTV camera (WV-BP550/G). After adding a droplet (3 µL) of ultrapure water on the sample surface, a photograph was immediately taken (at room temperature, 25 °C). For the WCA measurements above the LCST, the samples were first heated to 50 °C using a Peltier module (ZP9102, 51W/6A) and allowed to equilibrate for 10 min before adding the water droplet to the surface and capturing the image. The temperature was controlled by applying an electrical current to the Peltier cell using a source meter unit (Keithley 2425). An IR thermal imaging camera (FLIR i7) was used to monitor the biosensor surface temperature during the experiment. ImageJ software (Drop Analysis plugin) was employed to determine the contact angle of the water drop in contact with the pSi surface.

RESULTS AND DISCUSSION

Polymer composition and functionality can be easily tuned through the use of reversible-deactivation radical polymerization (RDRP) and orthogonal post-modification, enabling the modular construction of environmentally-responsive polymers displaying different recognition motifs. In this study, we used reversible addition-fragmentation chain-transfer (RAFT) polymerization to synthesize a functional copolymer based on *N*-isopropylacrylamide (NIPAm) and a protected acylhydrazide derived monomer. RAFT allows the copolymer molecular weight to be tailored, and produces polymers with functional chain ends which can be used for subsequent modification or surface attachment.[43] Briefly, the protected acylhydrazide derivative (*tert*-butyl 2-methacryloylhydrazine-1-carboxylate – **M1**) was copolymerized with

NIPAm (see Supporting Information, Scheme S1) to yield a polymer scaffold (**P1**) displaying approximately 71 NIPAm units and 14 protected acylhydrazide functionalities. The average molecular weight and dispersity of the copolymer were 10,800 g mol^{-1} and Đ= 1.09, respectively (Table S1, Figure S1, S2). Subsequent deprotection yields a polymer with pendant acylhydrazide units (**P2**), enabling modification with multiple copies of carbohydrate recognition motifs GM1os or lactose (**P2-GM1os** or **P2-Lac**, respectively) (Scheme 1). For the current systems, we performed differential scanning calorimetry (DSC) to investigate the thermoresponsive behavior of our copolymers in phosphate buffered saline (PBS: 137 mM NaCl, 2.7 mM KCl, 10 mM NaH_2PO_4, 1.8 mM KH_2PO_4) (Table S2, Figure S6). The carbohydrate-decorated polymers displayed a reversible phase transition, with a lower critical solution temperature (LCST) of 43.3 °C observed for **P2-Lac** and **P2-GM1os**, a slightly elevated value compared to that corresponding to the unmodified polymer scaffold, **P2** (40.8 °C). The phase transition was observed to occur over a broader temperature range in **P2-GM1os**, owing to the additional hydrogen bonding capability of the polymer upon modification with multiple pentasaccharide units.

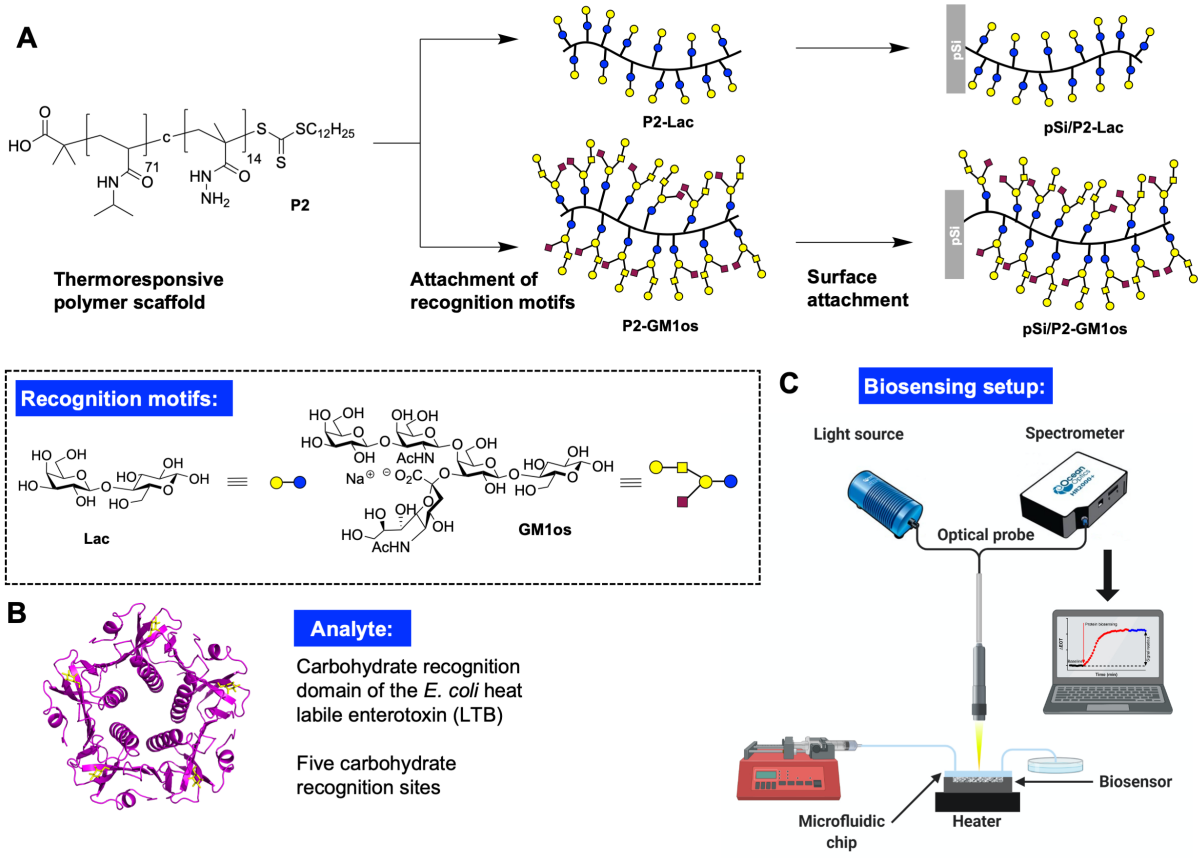

Scheme 1. Regenerable biosensing platform setup: (A) Thermoresponsive multivalent glycopolymer receptors are appended onto pSi. (B) The carbohydrate recognition domain of the *E. coli* heat-labile enterotoxin (LTB), shown complexed with five galactose residues (1LTA.pdb). (C) Experimental setup for LTB sensing using pSi interferometer.

With the polymeric receptors synthesized, we next produced pSi thin films with nanoscale pores from highly doped *p*-type silicon wafers via electrochemical anodization. Seven different conditions for fabricating the pSi interferometers (Table 1) were tested to determine the optimum pore size and pore depth for the best biosensing performance (as explained later). Further information on the fabrication parameters and the resulting morphological features (i.e., pore size, porosity and pore depth) can be found in the Supporting Information S2. In brief, an increase in the current density during anodization results in larger pore sizes

with cylindrical pore geometries, decreased side branching, and higher porosities. These trends agree with previously reported results.[44,45] Figure S7 shows typical outcomes of the SEM analysis performed on the top and cross-sections of the pSi surfaces we used going forward. We needed the surface of the pores to be open and large enough to allow for adequate surface functionalization in subsequent steps. The attachment of polymeric receptors **P2-Lac** and **P2-GM1os** (M_n 14,300 and 24,800 g mol^{-1}, respectively) required pores large enough to allow effective diffusion of the polymeric material into the porous network. Cross-section SEM images (Figure S7) demonstrated that the etching resulted in a column-like morphology. The depth of the pores is continuous from top to bottom through the thickness of the film. The overall pore depth (i.e., thickness of the film) can be adjusted accordingly by varying the anodization time and was 2.0 µm for Surfaces 1 to 5, and 1.6 µm and 3.1 µm for Surfaces 6 and 7, respectively (SEM not shown). We then used these pSi interferometers (Surfaces 1 to 7) to optimize the biosensor preparation.

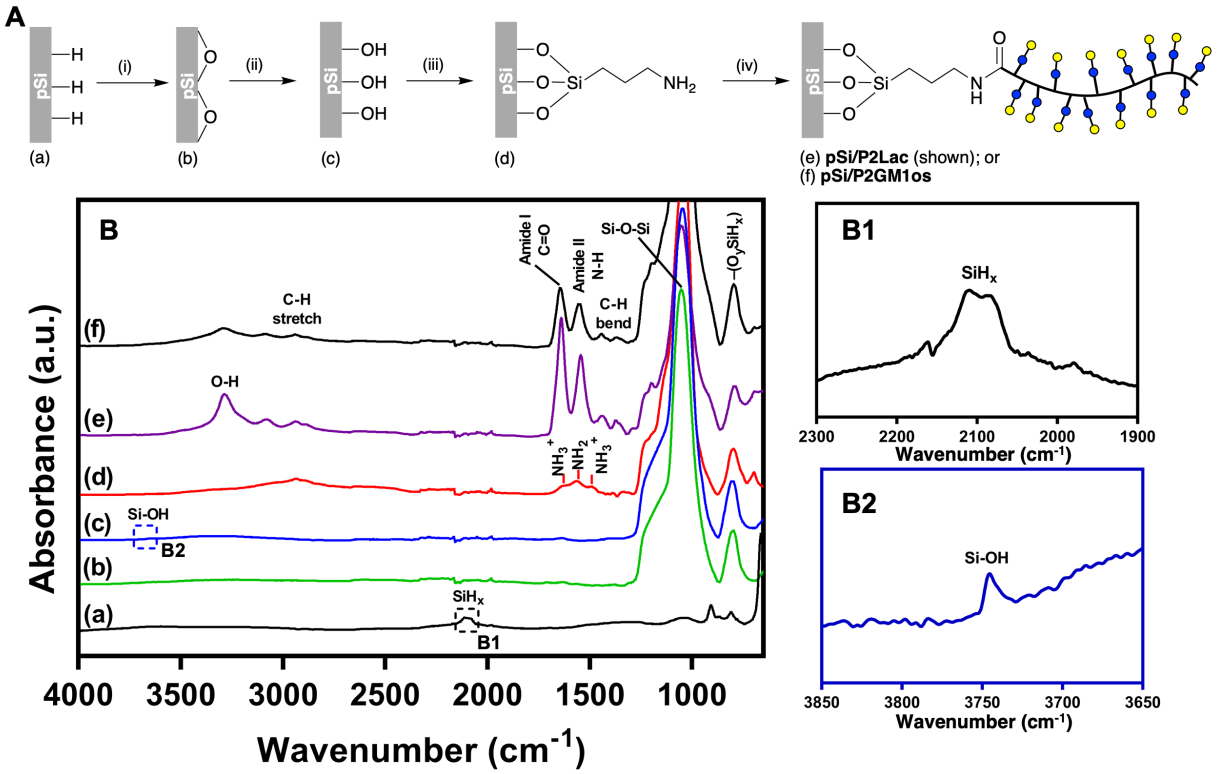

Figure 1. (A) Surface modification of pristine pSi surfaces with multivalent polymeric receptors: (i) thermal oxidation (600 ºC, 1 h); (ii) ozone oxidation, 30 min; (iii) APTMS, 10 min; (iv) **P2-Lac** or **P2-GM1os** grafting, EDC and NHS in MES buffer. (B) IR spectra overlays of (a) as-fabricated, (b) thermally-oxidized, (c) ozone-oxidized and, (d) APTMS-modified pSi surface; (e) **pSi/P2-Lac** and (f) **pSi/P2-GM1os** biosensor surface. Insets B1 and B2 show enlarged spectra for clarity.

To fabricate the biosensor, we needed to immobilize the polymer scaffold into the pores of the pSi interferometers. The as-anodized pSi surface was chemically modified prior to attaching either **P2-Lac** or **P2-GM1os** multivalent receptors (Figure 1A). Infrared spectroscopic analysis (Figure 1B) was used to verify the changes to the surface chemistry after each modification reaction step. Briefly, as-fabricated pSi produced characteristic peaks at 2110 and 2083 cm^{-1} corresponding to the Si-H_2 and Si-H stretching vibrations, respectively (Figure 1, inset B1). After thermal oxidation, the formation of Si back-bonds in the freshly etched pSi was observed as a broad peak at 1039 cm^{-1} that is related to Si–O–Si stretching mode in addition to the typical –(O_ySiH_x) mode at 801 cm^{-1}. [46,47] Thermally-oxidized pSi surfaces were further treated with ozone oxidation to produce silanol (Si–OH) groups evidenced by the apperance of the characteristic silanol peak at 3745 cm^{-1} [48,49] (Figure1, inset B2). This two-step oxidation approach was necessary to produce a surface less susceptible to hydrolytic attack when exposed to aqueous media and, at the same time, to promote the generation of enough silanol groups

to readily react to the methoxy groups of the silane.[50] Next, we introduced amino groups onto the oxidized pSi surface using aminopropyl trimethoxysilane (APTMS) resulting in the peaks found at 1410, 1498, 1565 and 1630 cm^{-1} corresponding to the CH_3 group of APTMS, symmetric $–NH_3^+$ deformation mode, NH_2 scissoring vibration mode, and the asymmetric $–NH_3^+$ deformation mode, respectively.[51] Afterward, either **P2-Lac** or **P2-GM1os** was covalently immobilized on the aminosilane-modified pSi surface via amide bond formation with the α-terminal carboxylic acids available in the receptors to produce the corresponding biosensor. IR bands assigned to amide II (N–H bending) and amide I (C=O stretching) were found at 1543 and 1640 cm^{-1} comfirming the attachment of the polymeric receptors into the pSi matrix. Additionally, the vibrational bands centered at 1441 and 1370 cm^{-1} are assigned to the symmetric methylene (CH_3 and CH_2) deformation modes of the sidechain and backbone while bands discernable in the range between 2850 and 3000 cm^{-1} are ascribed to C–H groups.[52] Finally, the broad band centered at 3283 cm^{-1} is ascribed to the hydrogen-bonded (O–H) stretching vibration, arising from the carbohydrate units appended onto the polymeric scaffold. Throughout the rest of this work, the fully functionalized pSi surfaces with our two multivalent polymeric receptors are referred to as **pSi/P2-Lac** and **pSi/P2-GM1os** biosensor, respectively.

Additionally, the surface modification was further corroborated using an FFT analysis of reflectivity spectra acquired from the pSi surface in air after each preparation step. FFT analysis allows the correlation of spectral shift experienced by the effective optical thickness peak (EOT = *2nL*) to the changes in the average refractive index (*n*) of pSi after each surface modification step. Figure S8A depicts the typical shifts in the spectral position of the EOT peak recorded after each functionalization step for one of our pSi surfaces. In fact, Figure S8B summarizes the overall positive differential EOT changes recorded during the sensor's preparation. The EOT value recorded upon oxidation of the pSi interferometers (i.e., EOT_{Ox}) was used as reference to produce the positive EOT changes. The consistent EOT changes observed after each functionalization step corroborate the IR analysis and the successful preparation of our biosensing platform.

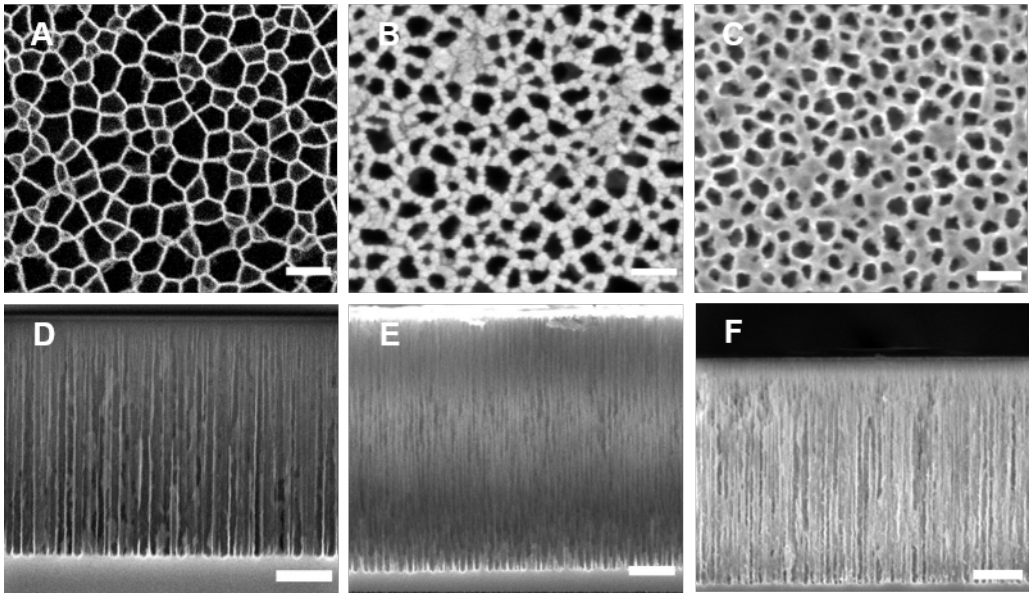

Figure 2. Top and cross-sectional SEM images for: (A and D) the as-fabricated pSi interferometer, (B and E) the **pSi/P2-Lac** biosensor and (C and F) the **pSi/P2-GM1os** biosensor. The pSi film was prepared using a current density of 41.6 mA cm^{-2} for 117 s (Table 1, Surface 4). The scale bars for the top and cross-sectional micrographs are 100 and 500 nm, respectively.

We used SEM to obtain a better understanding of the morphological changes to the pSi surfaces after polymer incorporation (Figure 2). Top and cross-sectional SEM images provide a visual comparison of the pristine (Figure 2 A and D), **P2-Lac** polymer-modified (Figure 2 B and E), **P2-GM1os** polymer-modified (Figure 2 C and F) pSi surfaces. Upon attachment of the polymers, the average pore diameter was reduced from 36 ± 14 nm for the pristine pSi film to 29 ± 16 and 25 ± 12 nm for the **pSi/P2-Lac** and **pSi/P2-GM1os**

biosensor surfaces, respectively (Figure 2 A-C; Figure S9). We will nonetheless demonstrate that the pore diameter remains accessible for the binding of LTB (58 kDa). The grafting of the **P2-Lac**/**P2-GM1os** polymers appears to uniformly decorate the pore walls rather than filling the internal volume of the pores throughout the entire depth of the pores (Figure 2 D-F).

With the polymer incorporated into the pSi interferometer, we have fabricated our biosensor for LTB detection through EOT changes. Before conducting our sensing experiments, we thoroughly investigated the stability of the polymer-modified pSi biosensor in aqueous environment. The stability against oxidation and corrosion in aqueous media is crucial given that we wanted to exploit the thermoresponsive properties of our polymer scaffold to regenerate the polymer surface after LTB binding to reuse the biosensor.

The silicon hydride-terminated surface of freshly prepared pSi films is highly reactive to atmospheric conditions (e.g., oxygen and water), leading to oxidation and hydrolytic corrosion of the porous scaffold. Oxidation causes a significant change in the effective refractive index (n) of the material (n = 3.5 for Si and n = 1.4 for SiO_2) and the EOT, interfering with the signal readout.[25] Similarly, corrosion can lead to changes in porosity and film thickness, reducing EOT, and leading to structural collapse and the loss of signal transduction.[48] A stabilized surface is therefore required when using pSi as the transduction element. We compared the stability of our polymer-modified pSi surfaces by exposure to PBS containing ethanol (5%, v/v) and NaOH solution (pH 12). The EOT value of the polymer-coated substrates is stable, and the surface displayed negligible EOT changes to suggest an effective capping of the pore walls (Figure S10). We expect the increased stability of the polymer-modified pSi film to stem primarily from the passivation of the pSi scaffold through the two-step (thermal and ozone) oxidation treatment associated with the preparation of the biosensors. Even in a more corrosive environment (pH 12), to accelerate the surface degradation in order to simulate the condition of long-term exposure in aqueous solution, which normally expedites pSi structural decay[48], the surface of the biosensors remained intact, as can be seen by the negligible changes in the EOT magnitude (Figure S10). This stability assay ensured a viable use of our modified pSi films as biosensors in aqueous media.

We used water contact angle (CA) measurements to qualitatively assess surface wettability properties of the different functionalization steps and the temperature-induced switching properties of our biosensors (Figure S11). Freshly etched pSi is hydride-terminated (Si–H), hydrophobic and highly reactive at room conditions.[53] A contact angle value of 104 ± 1.5° was obtained for as-fabricated pSi interferometers which are in accordance with those reported in the literature.[53,54]A discussed earlier, a simple method to stabilize pSi is oxidation, which generates a Si–OH capped surface with a thin oxide layer. Oxidation produced highly hydrophilic pSi surfaces with contact angles of 19 ± 0.6°, values in fair agreement with those found in the literature.[53,54] Surface hydroxyl groups were then reacted with APTMS silane, which further stabilizes the surface against hydrolytic attack and provides a means of grafting the carboxylic group (-COOH) of our polymers to the pore walls. Silanization resulted in a hydrophilic surface displaying an increased contact angle of 46 ± 3°. Finally, the polymer-modified pSi surfaces produced hydrophilic surfaces with a contact angle of about 61 ± 2.1°. These results further verify the successful surface modifications steps and reproducible preparation of our biosensors. To investigate the temperature-induced properties of our biosensor, we increased the temperature of the polymer-functionalized surfaces and we observed a contact angle increase from 61 ± 2.1° to 69 ± 2.8° after heating the surfaces above the LCST to 50 °C; this suggests an expected switch toward a more hydrophobic surface character due to the thermally induced de-solvation of the copolymer. De-solvation of NIPAm above its LCST leads to a volume phase transition from a coil-to-globule conformational structure. This transition is accompanied with the formation of a hydrophobic microenvironment from the collapse of the hydrated coil structures of NIPAm, which in turn influences the net wetting properties of the biosensor's surface, observed as a discernable increase in the contact angle magnitude upon heating due to the hydrophobicity of NIPAm. We believe that the distinct change in the contact angle of about 8 ° is an indicator of the thermoresponsiveness of our sensors. However, the contact angle difference obtained above and below the LCST of poly(NIPAm) for our platform is relatively small compared to other values reported in the literature for poly(NIPAm) brushes grafted to pSi surfaces.[35] We attribute the difference to stem mainly from the use of a "grafting to" rather than a "grafting from" technique for our polymer-grafting procedure, with the latter generating higher grafting densities and also to the related effect of the molecular weight of the polymer chains.[35,55] We also observed that the apparent LCST of the polymeric receptors grafted into the pores remains reasonably close to the temperature reported for our

polymers in solution (~43 °C). Minor variations in the cloud point of poly(NIPAm) have been observed when incorporated into nanostructured pSi surfaces but still remaining close to the LCST.[33,35,36] With the stability and stimulus-responsiveness confirmed, we moved on to assess the performance of our biosensor in the detection of LTB. Figure 3A shows the reflectivity spectrum of the **pSi/P2-Lac** surface before and after detection of LTB. Conspicuous variations in the position of the Fabry-Pérot interference fringes in the reflectivity spectrum were noted after detection of LTB in buffer (red trace, Figure 3A). The spectral displacement of these fringes towards larger wavelength values (i.e., redshift) with respect to their initial position in buffer (black trace, Figure 3A) represents evidence of the capture of LTB by the polymeric receptors within the pores. The latter is in line with previous observations[24,48], demonstrating a net increase in the effective refractive index of the pSi layer due to the occupation of the internal volume of the pores by the analyte. The sensor response can be made quantitative by processing the reflectivity spectrum of the sensing experiment using FFT analysis and presenting it as a sensorgram (i.e., EOT over time) (Figure 3B). Briefly, EOT = 2*nL* and the parameter therefore contains information about the effective refractive index (*n*) and the physical thickness (*L*) of the pSi interferometer. *L* remains constant and only *n* is susceptible to variation. Any change in *n* can be quantified and illustrated in the form of a sensorgram. A stable baseline was acquired in buffer (0 – 5 min) of a **pSi/P2-Lac** surface prepared using Surface 3 (Table 1), followed by the introduction of LTB at a subunit concentration of 120 µM (i.e., pentamer concentration of 24 µM) (6 – 22 min). A typical dose-response curve upon detection of LTB can be observed, causing a change in the magnitude of EOT (0% to 2.25% after 22 min). The observed trend is attributed to the fact that *n* of the pSi film increases upon capture of LTB. A rinsing step with buffer was applied to remove any unbound protein (23 – 30 min). The washing procedure was noted to cause a negligible change from 2.25 to 2.21% in the magnitude of EOT. This final value in EOT is then considered as the signal readout of our hybrid biosensor.

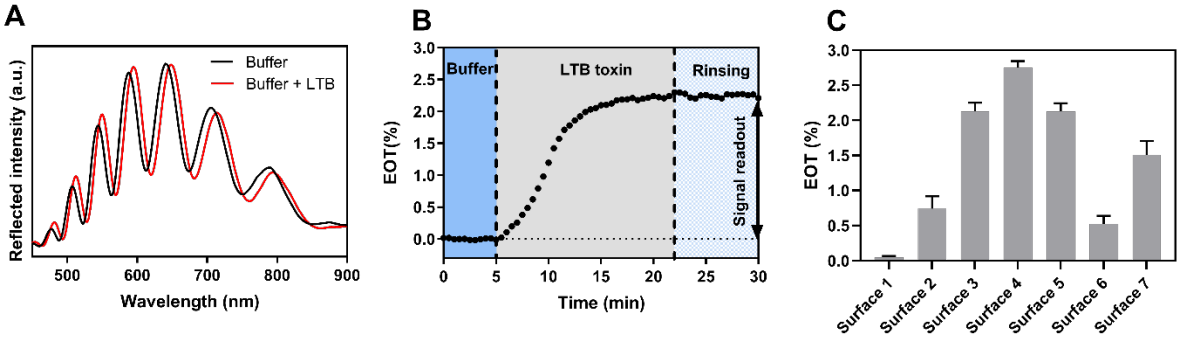

Figure 3. (A) Reflectivity spectrum of the biosensor surface (Table 1, Surface 4) collected in buffer solution before (black line) and after (red line) complexation of LTB, presented as a redshift in the reflectivity signature. (B) Typical sensorgram in response to LTB showing the change in the magnitude of EOT during the sensing experiment: a baseline was acquired in buffer, followed by the infusion of LTB. After rinsing steps to remove unbound protein, a stable signal readout was attained. (C) EOT signal readouts of different **pSi/P2-Lac** biosensors measured using FFT reflectance spectroscopy for seven different conditions of a pSi film (listed in Table 1), as a response to LTB (120 µM). Data are shown as mean ± SD, n = 3.

With the basic function of our biosensor confirmed, we moved on to optimize the sensor by investigating the influence of the pSi substrate morphology, i.e., pore size and thickness, using the different fabrication conditions listed in Table 1. Figure 3C presents the corresponding EOT changes after a typical biosensing experiment. Biosensing experiments were conducted at room temperature using a flow rate of 5 µL min^{-1} throughout the entire course of the experiment unless otherwise specified. Surfaces 1 to 5 (the number refers to the etching condition in Table 1) exhibit different pore sizes ranging from smaller (13 nm) to bigger (70 nm), with comparable pore depths (~2.0 µm). Relatively small pore sizes (13-25 nm, Surface 1) appear not to allow for LTB to access the pores after surface functionalization and hence limit the effect on EOT significantly, with EOT variation only being 0.05 ± 0.02%. Increasing the diameter of such pores allowed for LTB access, diffusion and binding within the pores, resulting in a clear readout. The sensitivity improved with increasing pore sizes from 0.74 ± 0.17% (19-28 nm, Surface 2) to 2.12 ± 0.12% (24-37 nm, Surface 3)

to 2.75 ± 0.09% (32-58 nm, Surface 4). Further increasing the pore size (37-70 nm, Surface 5) did not improve the sensitivity; in fact, if the pore diameter became too large, the sensitivity was reduced. While a higher internal pore volume enables easier access and diffusion of LTB into the pores to facilitate binding, when the pore volume becomes too big, the refractive index changes become less pronounced, and the effective EOT upon analyte binding is reduced, which renders the sensor less sensitive. To explore the effect of pore depth (i.e., thickness of the pSi interferometer) on the biosensor performance, we prepared two further sensors (Surface 6 and 7, Table 1) with varying pore depth by using the same procedure as for the sensor with the maximum readout (Surface 4) to maintain a comparable pore diameter. Reducing the pore length by 0.5 µm led to a significant reduction in sensitivity (0.52 ± 0.12%). Extending the pore length by almost 1.0 µm did not improve the sensitivity either (1.5 ± 0.2%). For thinner layers (< 2.0 µm), the fidelity of the optical interference pattern (i.e., fringes in the reflectivity spectrum) is undesirable and may negatively affect the magnitude of the EOT change. Whereas for thicker layers (> 3.0 µm), we hypothesize a hindered diffusion of LTB towards the bottom of the thicker layer as the main mass transfer limiting factor for our system. It is well-known that the porous layer thickness has an impact on the binding-rate of a biosensor, the latter decreasing for thicker pSi layers.[56]

We continued to use a biosensor based on Surface 4 to investigate the limit of detection (LOD) of our **pSi/P2-Lac** biosensor. We, therefore, established a calibration curve using FFT reflectance spectroscopy measurements on solutions containing different (subunit) concentrations of LTB ranging from 0 to 60 µM (i.e., LTB pentamer concentrations of 0 to 12 µM) (Figure 4A, solid symbols). The magnitude of EOT increased with increasing LTB concentration. We used a Hill function for the non-linear fitting of the experimental data:[57]

$$R = R_{max} \frac{[L]^{\alpha}}{{K_d}^{\alpha} + [L]^{\alpha}} \quad (3)$$

Herein, R is the change in the value of EOT of the biosensor to the LTB concentration [L], R_{max} is the maximal response signal at [L] → ∞ (i.e., saturation), α is the Hill coefficient and K_d is the dissociation constant. The Hill equation has been demonstrated to be useful for the description of biosensor calibration curves.[56,58–61] The apparent dissociation constant (K_d) obtained for our **pSi/P2-Lac** biosensor was of 42.12 ± 2.3 µM, describing the concentration at which half of the maximum signal is attained. The calculated value for the Hill coefficient was 1.0 ± 0.07. The Hill coefficient represents an interaction coefficient and in case of a (strong) positive cooperativity, it reflects the stoichiometry of ligand-receptor binding, with values approximately equal to 1.0 suggesting independent (non-cooperative) binding.[62] A sensitivity (S) of 0.032 ± 0.004% (EOT intensity per µM of LTB subunit) was calculated in the linear range of the concentration-dependent curve (Figure 4A, inset), corresponding to a theoretical LOD of 1.87 µM (indicated by the gray area in Figure 4A) defined as $3\sigma_{EOT0}/S$, where σ_{EOT0} (2.0 x 10^{-2}%) is the standard deviation of EOT values measured during baseline establishment and incubation of the biosensor in buffer (i.e., 0 µM of LTB), and S is the biosensor sensitivity.

To further improve the performance of our system, polymer-modified pSi biosensors prepared using the **P2-GM1os** polymeric receptors, were fabricated. The pentasaccharide unit of the GM1 ganglioside, the GM1 oligosaccharide (GM1os), has been demonstrated by isothermal titration calorimetry to display nanomolar affinity towards CTB.[5] Thereby, we envisage that the multiple copies of the GM1os recognition motif attached onto our polymeric scaffold could boost the sensitivity of the platform, improving the LOD for LTB, the *E. coli* analogue of CTB. Thus, we prepared a calibration curve for different (subunit) concentrations of LTB in solution ranging from 0 to 50 µM (i.e., pentamer concentration of 0 to10 µM) (Figure 4B). The magnitude of EOT increased with increasing LTB concentration. The experimental data were fitted using the Hill function resulting in a Hill coefficient of 0.69 ± 0.09, and an apparent K_d of 4.5 ± 0.97 µM. A sensitivity (S) of 0.185 ± 0.001% (EOT intensity per µM of LTB subunit) was calculated in the linear range of the concentration-dependent curve (Figure 4B, inset), corresponding to a LOD of 0.135 ± 0.02 µM, which is at least one order of magnitude lower than the LOD obtained using the **pSi/P2-Lac** biosensor. Typical sensorgrams presenting the optical response as the variation in EOT toward

complexation of different (subunit) concentrations of LTB for a **pSi/P2-Lac** and a **pSi/P2-GM1os** biosensor (and corresponding experimental details) are shown in Figure S12 A and B, respectively.

To assess the extent of non-specific binding of proteins and lectins to our biosensing platform, we used various concentrations of streptavidin (SA, 54.3 kDa) ranging from 0 to 60 μM for the preparation of a calibration curve to corroborate the selectivity of our biosensor (Figure 4A, open circle). SA has no appreciable binding affinity towards the recognition motifs appended onto the polymeric scaffold and is of a similar molecular weight to our target analyte. An EOT value of 0.08 ± 0.04% was obtained for the highest concentration of SA (60 μM). Interestingly, the readouts measured for the rest of the concentrations of SA fall well below the $3\sigma_{EOT0}$ noise level recorded in buffer for our biosensor. In addition, succinyl-concanavalin A (s-Con A,), a modified lectin with affinity to terminal α-D-mannosyl and α-D-glucosyl residues of several glycoproteins was also used as a carbohydrate-binding molecule for non-specific binding control tests. Chemical derivatization of tetrameric concanavalin A (Con A, ~102 kDa) with succinic anhydride converts the protein to a dimeric molecule with a molecular weight of ~51 kDa without altering its carbohydrate-binding affinity;[63] molecular weight comparable to that of LTB (refer to concanavalin A modification protocol in SI). Concentrations of s-Con A in the range of 65 and 55 μM (solid triangle, Figure 4) were tested using each of the biosensors, respectively. EOT values of 0.07 ± 0.04 and 0.04 ± 0.03% were obtained for the **pSi/P2-Lac** and **pSi/P2-GM1os**, respectively. These values are at least one order of magnitude lower than the EOT readouts obtained for the highest concentration tested with each biosensor.

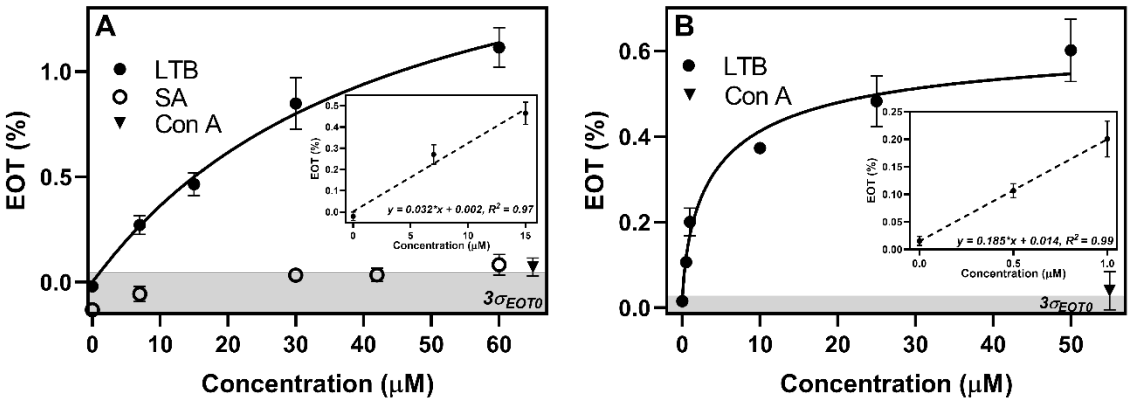

Figure 4. Dose-response curves expressed as the variation in EOT for different LTB subunit (solid circle) and nonspecific proteins (SA, open circle; s-Con A, solid triangle) concentrations tested using (A) the **pSi/P2-Lac** and (B) the **pSi/P2-GM1os** biosensors. Experimental data were fitted using Hill function (solid line). A linear regression (insets, dashed line) was performed in the linear range of both concentration-dependent curves to calculate the sensitivity and limit of detection of each biosensor. The gray area in the graphs represents the $3\sigma_{EOT0}$ noise level recorded in buffer for each biosensor. Data are shown as mean ± SD, n = 3 (for some points, the error bars are shorter than the height of the symbol).

Lastly, with the ability of our system to detect LTB confirmed, we explored the thermoresponsive functionality of these receptors towards a reversible complexation of LTB. We observed that, below their LCST, polymeric receptors complex LTB with micromolar affinity. When the temperature is increased above their LCST, polymers undergo a reversible coil-to-globule structural transition, rendering a proportion of the lactose/GM1os recognition motifs inaccessible to LTB and restricting the interaction of the polymer with the protein.[21] We hypothesized that a change in external temperature could be harnessed to modulate the overall avidity of our polymeric material for LTB. In our reversibility experiments, a **pSi/P2-Lac** biosensor was exposed to LTB (at room temperature, R.T.) followed by thermal cycling (50 °C) to study 'catch-and-release' of LTB and the regeneration of the sensor when the system was allowed to cool to R.T. These temperatures values were chosen to be well below and well above the solution LCST (43.3 °C) of the **P2-**

Lac material, whilst not sufficiently high to disrupt recognition through denaturation of the protein. The obtained sensorgram summarizes the real-time characteristic curves of the biosensor regeneration experiments (Figure 5A). The experiment was run for two consecutive regeneration cycles. Reflectivity spectra were collected as a function of time during the entire course of the experiment and processed using FFT reflectance spectroscopy yielding the EOT sensorgram (Figure 5A). The observed differences in the magnitude of EOT are produced either by complexation of LTB or by temperature-dependent structural transitions of the immobilized polymeric receptors.

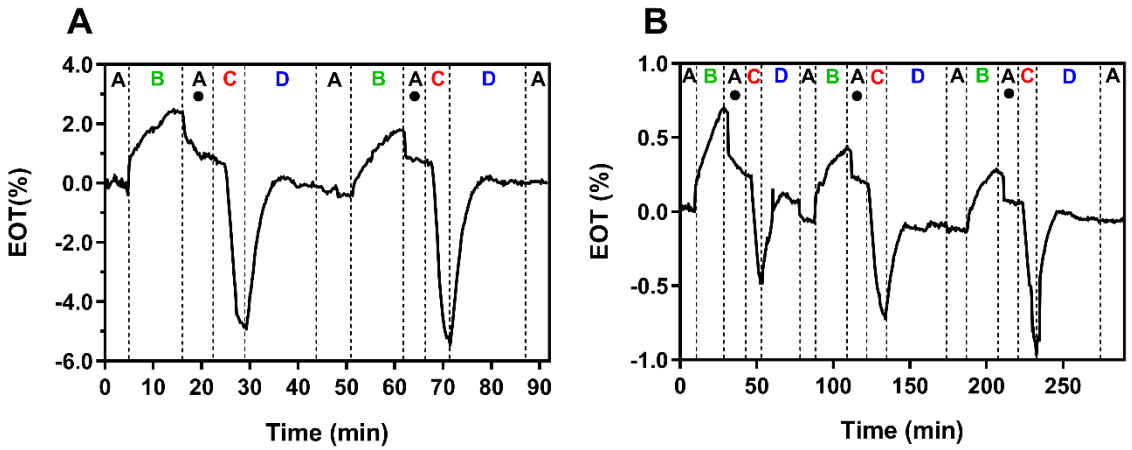

Figure 5. (A) EOT sensorgram obtained upon exposure of the **pSi/P2-Lac** biosensor to LTB (60 μM subunit concentration) in two consecutive temperature-dependent reversible cycles, (B) EOT variation for the 'catch-and-release' behavior of the **pSi/P2-GM1os** biosensor upon complexation of LTB (5.0 μM subunit concentration) for three consecutive temperature-dependent reversible cycles. A, B, C and D indicate incubation with PBS buffer (R.T.), with LTB (R.T.), with PBS upon heating cycle (from R.T. to 50 °C) and with PBS upon cooling cycle (from 50 °C to R.T.), respectively. (●) indicates the time points at which the signal readouts were attained for each biosensor.

The sensorgram depicts an initial baseline acquired in PBS buffer at R.T. (time point A), followed by the infusion of LTB (60 μM subunit concentration) at R.T., producing a dose-response behavior in the magnitude of EOT upon recognition of LTB (time point B). Removal of unbound protein (rinsing step, time point A) produced a first stable signal readout. Upon heating, a significant decrease in the magnitude of EOT was observed as temperature increased from R.T. to 50 °C (time point C). We attribute this abrupt negative decrease in the EOT magnitude to the combined effect of the depletion of LTB in the receptors and the thermally-triggered de-solvation of **P2-Lac** (i.e., coil-to-globule structural transition) at temperatures above LCST. De-solvation of **P2-Lac** likely results in a significant proportion of the carbohydrate recognition units being buried inside the collapsed globule, restricting interaction with binding sites on LTB. In addition, and consistent with the literature,[36,64] since the NIPAm component of the **P2-Lac** material is rendered hydrophobic above its LCST, the abrupt decrease in EOT observed for the **pSi/P2-Lac** hybrid upon heating, could be explained in terms of ejection of solution (i.e., buffer) from the polymeric material and the nanopores, yielding to a net reduction in the average refractive index of the porous matrix, which prevails over the increase in the refractive index of poly(NIPAm). When the system is cycled back to R.T., the behavior of the hybrid surface is reversed, as demonstrated by a continuous increase in the magnitude of EOT, approaching its initial baseline value (time point D). This behavior correlates the reversibility and relative complete regeneration of the polymer within the pores by generating a new stable baseline (time point A) after two consecutive cycles of use. Furthermore, the EOT values for the signal readouts attained (●, Figure 5A) were of 0.9 and 1.08%, for the first and second cycle, respectively, proving fairly good reproducibility. In addition, a reversibility experiment performed using the **pSi/P2-GM1os** biosensor resulted in the sensorgram presented in Figure 5B. The biosensor was exposed to three consecutive regeneration cycles upon complexation of LTB (5.0 μM subunit concentration). As explained, the observed changes in EOT are due to the complexation of LTB, or the temperature-dependent structural transition of

the NIPAm component of the **P2-GM1os** receptors. One of the advantages of using the **pSi-P2-GM1os** biosensor is its high-affinity to LTB (i.e., sub-micromolar range). The signal readouts obtained for each of the three consecutive cycles were of 0.249, 0.245 and 0.187%, respectively (●, Figure 5B). In order to obtain comparable readings from the biosensor due to the underlying drift towards lower EOT values observed in the sensorgram (Figure 5B), the readouts for each cycle were calculated by adding the absolute value of the average EOT obtained for each of the baselines (before the introduction of LTB) to the readout value attained after washing off the unbound protein. We attribute this drift in biosensor's response to two main possibilities, one being the detachment of the polymeric receptors throughout the course of the experiment and, the second, to the time-dependent dissolution of the pSi scaffold.[47] Nevertheless, we observed a good reproducibility of the EOT values obtained for the first two consecutive regeneration cycles. We hypothesize that the difference of 0.053% observed in the signal readout for the third cycle (compared to the EOT values of the first two cycles) is due to a proportion of polymeric receptors which are unable to regenerate after thermal cycling. This observation suggests that some polymeric receptors remained in a globule-like conformational structure for the duration of this detection-regeneration cycle, thus decreasing the availability of these receptors for a new 'catch' of LTB. Nevertheless, these results demonstrate effective 'catch-and-release' behavior for two consecutive cycles of use with high reproducibility.

CONCLUSIONS

Two different multivalent polymeric receptors were synthesized for complexation of LTB toxin. Receptors comprised of a temperature-responsive poly(NIPAm) scaffold with carbohydrate recognition motifs (lactose or GM1os) appended onto the polymer. Hybrid biosensors were prepared by incorporating these receptors into different pSi nanostructured surfaces displaying distinct morphological properties (namely pore size, porosity and thickness) in order to identify the superior biosensing performance. The observed optical response of these hybrid materials was found to be highly dependent on the nanostructured template used as the interferometric transducer. Our label-free optical biosensor shows low micromolar affinity towards LTB for the **pSi/P2-Lac** biosensor, whereas a sub-micromolar affinity was achieved for the **pSi/P2-GM1os** biosensor. Reproducible signal readouts were attained within a time frame of 30 and 60 min for each biosensor, respectively. Additionally, the stimulus-responsive character of the receptors was demonstrated to modulate their affinity and avidity for LTB in response to changes in the temperature of the surrounding medium, rendering them capable of 'catch-and-release' behavior with high reproducibility for two consecutive readings. This thermally-driven mechanism has been exploited to reversibly complex LTB with nearly complete regeneration of the biosensor for subsequent re-use.

By building on these results, we anticipate that our system could contribute to the development of point-of-care (POC) diagnostic tools for a variety of diarrheal diseases caused by bacterial toxins such as cholera, travelers' diarrhea and dysentery, by providing a temperature-mediated platform to conveniently detect the presence of a toxin, and a means to isolate the analyte for further identification if required. The analogous cholera toxin can be been detected in the watery diarrhoea of infected patients at pM-nM concentrations by ELISA assays.[65] Optical detection methods are well suited to the analysis of such samples, as they are insensitive to variation in parameters such as colour and ionic strength. The sample concentration required to enable the use of our platform could be achieved rapidly using techniques such as cross-flow filtration, which could be incorporated into our microfluidic device. Our methodology could be easily adapted to other disease-related proteins by varying the carbohydrate recognition motif attached to the polymer scaffold, presenting a versatile route to the development of new diagnostics.

ASSOCIATED CONTENT

The Supporting Information contains further details on the synthesis, fabrication and characterization of the polymers, the porous silicon interferometers and the hybrid biosensors.

AUTHOR INFORMATION

Corresponding Authors

*E-mail: markus.muellner@sydney.edu.au; nicolas.voelcker@monash.edu

Notes

The authors declare no competing financial interest.

ACKNOWLEDGMENTS
This work was performed in part at the Melbourne Centre for Nanofabrication (MCN) in the Victorian Node of the Australian National Fabrication Facility (ANFF). E.E.A. thanks for the postdoctoral fellowships granted by CONACyT (CVU 336883, call number 291121 and 291231). C.S.M. is a grateful recipient of a Marie Skłodowska-Curie Global Fellowship; this project has received funding from the European Union's Horizon 2020 research and innovation programme under the Marie Sklodowska-Curie grant agreement No. 702927. C.S.M. thanks Professor W. Bruce Turnbull (University of Leeds, UK) for kindly providing bacterial cell stocks used to express proteins for this work. M.M. acknowledges the Australian Research Council (DE180100007) for funding. TOC (Table of Content Graphic) and panel C (from Scheme 1) were created with Biorender.com.

REFERENCES

(1) Bain, R.; Cronk, R.; Hossain, R.; Bonjour, S.; Onda, K.; Wright, J.; Yang, H.; Slaymaker, T.; Hunter, P.; Prüss-Ustün, A.; Bartram, J. Global Assessment of Exposure to Faecal Contamination through Drinking Water Based on a Systematic Review. *Trop. Med. Int. Health* **2014**, *19* (8), 917–927.

(2) Troeger, C.; Blacker, B. F.; Khalil, I. A.; Rao, P. C.; Cao, S.; Zimsen, S. R. M.; Albertson, S. B.; Stanaway, J. D.; Deshpande, A.; Abebe, Z.; Alvis-Guzman, N.; Amare, A. T.; Asgedom, S. W.; Anteneh, Z. A.; Antonio, C. A. T.; Aremu, O.; Asfaw, E. T.; Atey, T. M.; Atique, S.; Avokpaho, E. F. G. A.; Awasthi, A.; Ayele, H. T.; Barac, A.; Barreto, M. L.; Bassat, Q.; Belay, S. A.; Bensenor, I. M.; Bhutta, Z. A.; Bijani, A.; Bizuneh, H.; Castañeda-Orjuela, C. A.; Dadi, A. F.; Dandona, L.; Dandona, R.; Do, H. P.; Dubey, M.; Dubljanin, E.; Edessa, D.; Endries, A. Y.; Eshrati, B.; Farag, T.; Feyissa, G. T.; Foreman, K. J.; Forouzanfar, M. H.; Fullman, N.; Gething, P. W.; Gishu, M. D.; Godwin, W. W.; Gugnani, H. C.; Gupta, R.; Hailu, G. B.; Hassen, H. Y.; Hibstu, D. T.; Ilesanmi, O. S.; Jonas, J. B.; Kahsay, A.; Kang, G.; Kasaeian, A.; Khader, Y. S.; Khalil, I. A.; Khan, E. A.; Khan, M. A.; Khang, Y.-H.; Kissoon, N.; Kochhar, S.; Kotloff, K. L.; Koyanagi, A.; Kumar, G. A.; Magdy Abd El Razek, H.; Malekzadeh, R.; Malta, D. C.; Mehata, S.; Mendoza, W.; Mengistu, D. T.; Menota, B. G.; Mezgebe, H. B.; Mlashu, F. W.; Murthy, S.; Naik, G. A.; Nguyen, C. T.; Nguyen, T. H.; Ningrum, D. N. A.; Ogbo, F. A.; Olagunju, A. T.; Paudel, D.; Platts-Mills, J. A.; Qorbani, M.; Rafay, A.; Rai, R. K.; Rana, S. M.; Ranabhat, C. L.; Rasella, D.; Ray, S. E.; Reis, C.; Renzaho, A. M. N.; Rezai, M. S.; Ruhago, G. M.; Safiri, S.; Salomon, J. A.; Sanabria, J. R.; Sartorius, B.; Sawhney, M.; Sepanlou, S. G.; Shigematsu, M.; Sisay, M.; Somayaji, R.; Sreeramareddy, C. T.; Sykes, B. L.; Taffere, G. R.; Topor-Madry, R.; Tran, B. X.; Tuem, K. B.; Ukwaja, K. N.; Vollset, S. E.; Walson, J. L.; Weaver, M. R.; Weldegwergs, K. G.; Werdecker, A.; Workicho, A.; Yenesew, M.; Yirsaw, B. D.; Yonemoto, N.; El Sayed Zaki, M.; Vos, T.; Lim, S. S.; Naghavi, M.; Murray, C. J. L.; Mokdad, A. H.; Hay, S. I.; Reiner, R. C. Estimates of the Global, Regional, and National Morbidity, Mortality, and Aetiologies of Diarrhoea in 195 Countries: A Systematic Analysis for the Global Burden of Disease Study 2016. *Lancet Infect. Dis.* **2018**, *18* (11), 1211–1228.

(3) Merritt, E. A.; Hol, W. G. AB5 Toxins. *Curr. Opin. Struct. Biol.* **1995**, *5* (2), 165–171.

(4) Branson, T. R.; Turnbull, W. B. Bacterial Toxin Inhibitors Based on Multivalent Scaffolds. *Chem. Soc. Rev.* **2013**, *42* (11), 4613–4622.

(5) Turnbull, W. B.; Precious, B. L.; Homans, S. W. Dissecting the Cholera Toxin−Ganglioside GM1 Interaction by Isothermal Titration Calorimetry. *J. Am. Chem. Soc.* **2004**, *126* (4), 1047–1054.

(6) Bernardi, A.; Jiménez-Barbero, J.; Casnati, A.; De Castro, C.; Darbre, T.; Fieschi, F.; Finne, J.; Funken, H.; Jaeger, K. E.; Lahmann, M.; Lindhorst, T. K.; Marradi, M.; Messner, P.; Molinaro, A.; Murphy, P. V.; Nativi, C.; Oscarson, S.; Penadés, S.; Peri, F.; Pieters, R. J.; Renaudet, O.; Reymond, J. L.; Richichi, B.; Rojo, J.; Sansone, F.; Schäffer, C.; Turnbull, W. B.; Velasco-Torrijos, T.; Vidal, S.; Vincent, S.; Wennekes, T.; Zuilhof, H.; Imberty, A. Multivalent Glycoconjugates as Anti-

Pathogenic Agents. *Chem. Soc. Rev.* **2013**, *42* (11), 4709–4727.

(7) Pukin, A. V; Branderhorst, H. M.; Sisu, C.; Weijers, C. A. G. M.; Gilbert, M.; Liskamp, R. M. J.; Visser, G. M.; Zuilhof, H.; Pieters, R. J. Strong Inhibition of Cholera Toxin by Multivalent GM1 Derivatives. *ChemBioChem* **2007**, *8* (13), 1500–1503.

(8) Branson, T. R.; McAllister, T. E.; Garcia-Hartjes, J.; Fascione, M. A.; Ross, J. F.; Warriner, S. L.; Wennekes, T.; Zuilhof, H.; Turnbull, W. B. A Protein-Based Pentavalent Inhibitor of the Cholera Toxin B-Subunit. *Angew. Chem., Int. Ed.* **2014**, *53* (32), 8323–8327.

(9) Zhang, Z.; Merritt, E. A.; Ahn, M.; Roach, C.; Hou, Z.; Verlinde, C. L. M. J.; Hol, W. G. J.; Fan, E. Solution and Crystallographic Studies of Branched Multivalent Ligands That Inhibit the Receptor-Binding of Cholera Toxin. *J. Am. Chem. Soc.* **2002**, *124* (44), 12991–12998.

(10) Mahon, C. S.; Fascione, M. A.; Sakonsinsiri, C.; McAllister, T. E.; Bruce Turnbull, W.; Fulton, D. A. Templating Carbohydrate-Functionalised Polymer-Scaffolded Dynamic Combinatorial Libraries with Lectins. *Org. Biomol. Chem.* **2015**, *13* (9), 2756–2761.

(11) Zeng, X.; Qu, K.; Rehman, A. Glycosylated Conductive Polymer: A Multimodal Biointerface for Studying Carbohydrate-Protein Interactions. *Acc. Chem. Res.* **2016**, *49* (9), 1624–1633.

(12) Park, S.; Gildersleeve, J. C.; Blixt, O.; Shin, I. Carbohydrate Microarrays. *Chem. Soc. Rev.* **2013**, *42* (10), 4310–4326.

(13) Otten, L.; Vlachou, D.; Richards, S. J.; Gibson, M. I. Glycan Heterogeneity on Gold Nanoparticles Increases Lectin Discrimination Capacity in Label-Free Multiplexed Bioassays. *Analyst* **2016**, *141* (14), 4305–4312.

(14) Fais, M.; Karamanska, R.; Allman, S.; Fairhurst, S. A.; Innocenti, P.; Fairbanks, A. J.; Donohoe, T. J.; Davis, B. G.; Russell, D. A.; Field, R. A. Surface Plasmon Resonance Imaging of Glycoarrays Identifies Novel and Unnatural Carbohydrate-Based Ligands for Potential Ricin Sensor Development. *Chem. Sci.* **2011**, *2* (10), 1952–1959.

(15) Hushegyi, A.; Bertok, T.; Damborsky, P.; Katrlik, J.; Tkac, J. An Ultrasensitive Impedimetric Glycan Biosensor with Controlled Glycan Density for Detection of Lectins and Influenza Hemagglutinins. *Chem. Commun.* **2015**, *51* (35), 7474–7477.

(16) Kale, R. R.; McGannon, C. M.; Fuller-Schaefer, C.; Hatch, D. M.; Flagler, M. J.; Gamage, S. D.; Weiss, A. A.; Iyer, S. S. Differentiation between Structurally Homologous Shiga 1 and Shiga 2 Toxins by Using Synthetic Glycoconjugates. *Angew. Chem., Int. Ed.* **2008**, *47* (7), 1265–1268.

(17) Won, S.; Richards, S. J.; Walker, M.; Gibson, M. I. Externally Controllable Glycan Presentation on Nanoparticle Surfaces to Modulate Lectin Recognition. *Nanoscale Horiz.* **2017**, *2* (2), 106–109.

(18) Pasparakis, G.; Cockayne, A.; Alexander, C. Control of Bacterial Aggregation by Thermoresponsive Glycopolymers. *J. Am. Chem. Soc.* **2007**, *129* (36), 11014–11015.

(19) Paul, T. J.; Rübel, S.; Hildebrandt, M.; Strzelczyk, A. K.; Spormann, C.; Lindhorst, T. K.; Schmidt, S. Thermosensitive Display of Carbohydrate Ligands on Microgels for Switchable Binding of Proteins and Bacteria. *ACS Appl. Mater. Interfaces* **2019**, *11* (30), 26674–26683.

(20) Paul, T. J.; Strzelczyk, A. K.; Feldhof, M. I.; Schmidt, S. Temperature-Switchable Glycopolymers and Their Conformation-Dependent Binding to Receptor Targets. *Biomacromolecules* **2020**, *21* (7), 2913–2921.

(21) Mahon, C. S.; Wildsmith, G. C.; Haksar, D.; De Poel, E.; Beekman, J. M.; Pieters, R. J.; Webb, M. E.; Turnbull, W. B. A “catch-and-Release” Receptor for the Cholera Toxin. *Faraday Discuss.* **2019**, *219*, 112–127.

(22) Arshavsky-Graham, S.; Massad-Ivanir, N.; Segal, E.; Weiss, S. Porous Silicon-Based Photonic Biosensors: Current Status and Emerging Applications. *Anal. Chem.* **2019**, *91* (1), 441–467.

(23) Lin, V. S. Y.; Motesharei, K.; Dancil, K. P. S.; Sailor, M. J.; Ghadiri, M. R. A Porous Silicon-Based Optical Interferometric Biosensor. *Science* **1997**, *278* (5339), 840–843.

(24) Pacholski, C.; Sartor, M.; Sailor, M. J.; Cunin, F.; Miskelly, G. M. Biosensing Using Porous Silicon Double-Layer Interferometers: Reflective Interferometric Fourier Transform Spectroscopy. *J. Am. Chem. Soc.* **2005**, *127* (33), 11636–11645.

(25) Kilian, K. A.; Böcking, T.; Gooding, J. J. The Importance of Surface Chemistry in Mesoporous Materials: Lessons from Porous Silicon Biosensors. *Chem. Commun.* **2009**, No. 6, 630–640.

(26) Jenie, S. N. A.; Pace, S.; Sciacca, B.; Brooks, R. D.; Plush, S. E.; Voelcker, N. H. Lanthanide Luminescence Enhancements in Porous Silicon Resonant Microcavities. *ACS Appl. Mater. Interfaces* **2014**, *6* (15), 12012–12021.

(27) Gaur, G.; Koktysh, D. S.; Weiss, S. M. Immobilization of Quantum Dots in Nanostructured Porous Silicon Films: Characterizations and Signal Amplification for Dual-Mode Optical Biosensing. *Adv. Funct. Mater.* **2013**, *23* (29), 3604–3614.

(28) Massad-Ivanir, N.; Bhunia, S. K.; Raz, N.; Segal, E.; Jelinek, R. Synthesis and Characterization of a Nanostructured Porous Silicon/Carbon Dot-Hybrid for Orthogonal Molecular Detection. *NPG Asia Mater.* **2018**, *10* (1), e463–e463.

(29) Mariani, S.; Paghi, A.; La Mattina, A. A.; Debrassi, A.; Dähne, L.; Barillaro, G. Decoration of Porous Silicon with Gold Nanoparticles via Layer-by-Layer Nanoassembly for Interferometric and Hybrid Photonic/Plasmonic (Bio)Sensing. *ACS Appl. Mater. Interfaces* **2019**, *11* (46), 43731–43740.

(30) Krepker, M. A.; Segal, E. Porous Silicon Polymer Composites. In *Handbook of Porous Silicon*; Canham, L., Ed.; Springer International Publishing: Cham, 2018; pp 269–280.

(31) Vasani, R.; Cole, M.; Ellis, A. V.; Voelcker, N. H. Stimulus-Responsive Polymers at Nanointerfaces. In *Nanotechnologies for the Life Sciences*; Kumar, C. S. S. R., Ed.; Wiley-VCH: Weinheim,Germany, 2011; Vol. 10, pp 59–103.

(32) McInnes, S. J. P.; Voelcker, N. H. Silicon-Polymer Hybrid Materials for Drug Delivery. *Future Med. Chem.* **2009**, *1* (6), 1051–1074.

(33) Segal, E.; Perelman, L. a.; Cunin, F.; Di Renzo, F.; Devoisselle, J. M.; Li, Y. Y.; Sailor, M. J. Confinement of Thermoresponsive Hydrogels in Nanostructured Porous Silicon Dioxide Templates. *Adv. Funct. Mater.* **2007**, *17* (7), 1153–1162.

(34) Segal, E.; Perelman, L. A.; Moore, T.; Kesselman, E.; Sailor, M. J. Grafting Stimuli-Responsive Polymer Brushes to Freshly-Etched Porous Silicon. *Phys. Status Solidi C* **2009**, *6* (7), 1717–1720.

(35) Vasani, R. B.; McInnes, S. J. P.; Cole, M. A.; Jani, A. M. M.; Ellis, A. V.; Voelcker, N. H. Stimulus-Responsiveness and Drug Release from Porous Silicon Films ATRP-Grafted with Poly(N-Isopropylacrylamide). *Langmuir* **2011**, *27* (12), 7843–7853.

(36) Pace, S.; Vasani, R. B.; Cunin, F.; Voelcker, N. H. Study of the Optical Properties of a Thermoresponsive Polymer Grafted onto Porous Silicon Scaffolds. *New J. Chem.* **2013**, *37* (1), 228–235.

(37) McInnes, S. J. P.; Szili, E. J.; Al-Bataineh, S. A.; Vasani, R. B.; Xu, J.; Alf, M. E.; Gleason, K. K.; Short, R. D.; Voelcker, N. H. Fabrication and Characterization of a Porous Silicon Drug Delivery System with an Initiated Chemical Vapor Deposition Temperature-Responsive Coating. *Langmuir* **2016**, *32* (1), 301–308.

(38) Tamarov, K.; Xu, W.; Osminkina, L.; Zinovyev, S.; Soininen, P.; Kudryavtsev, A.; Gongalsky, M.; Gaydarova, A.; Närvänen, A.; Timoshenko, V.; Lehto, V. P. Temperature Responsive Porous Silicon Nanoparticles for Cancer Therapy – Spatiotemporal Triggering through Infrared and Radiofrequency Electromagnetic Heating. *J. Controlled Release* **2016**, *241*, 220–228.

(39) Kilian, K. A.; Böcking, T.; Gaus, K.; King-Lacroix, J.; Gal, M.; Gooding, J. J. Hybrid Lipid Bilayers in Nanostructured Silicon: A Biomimetic Mesoporous Scaffold for Optical Detection of Cholera Toxin. *Chem. Commun.* **2007**, No. 19, 1936–1938.

(40) Lai, J. T.; Filla, D.; Shea, R. Functional Polymers from Novel Carboxyl-Terminated Trithiocarbonates as Highly Efficient RAFT Agents. *Macromolecules* **2002**, *35* (18), 6754–6756.

(41) Leece, R.; Hirst, T. R. Expression of the B Subunit of Escherichia Coli Heat-Labile Enterotoxin in a Marine Vibrio and in a Mutant That Is Pleiotropically Defective in the Secretion of Extracellular Proteins. *Microbiology* **1992**, *138* (4), 719–724.

(42) Tong, Z.; Rajeev, G.; Guo, K.; Ivask, A.; McCormick, S.; Lombi, E.; Priest, C.; Voelcker, N. H. Microfluidic Cell Microarray Platform for High Throughput Analysis of Particle-Cell Interactions. *Anal. Chem.* **2018**, *90* (7), 4338–4347.

(43) Willcock, H.; O'Reilly, R. K. End Group Removal and Modification of RAFT Polymers. *Polym. Chem.* **2010**, *1* (2), 149–157.

(44) Herino, R. Porosity and Pore Size Distributions of Porous Silicon Layers. *J. Electrochem. Soc.* **1987**, *134* (8), 1994.

(45) Zhang, X. G. Morphology and Formation Mechanisms of Porous Silicon. *J. Electrochem. Soc.* **2004**, *151* (1), C69.

(46) Salonen, J.; Lehto, V. P. Fabrication and Chemical Surface Modification of Mesoporous Silicon for Biomedical Applications. *Chem. Eng. J.* **2008**, *137* (1), 162–172.

(47) Shtenberg, G.; Massad-Ivanir, N.; Fruk, L.; Segal, E. Nanostructured Porous Si Optical Biosensors: Effect of Thermal Oxidation on Their Performance and Properties. *ACS Appl. Mater. Interfaces* **2014**, *6* (18), 16049–16055.

(48) Janshoff, A.; Dancil, K.-P. S.; Steinem, C.; Greiner, D. P.; Lin, V. S. Y.; Gurtner, C.; Montesharei, K.; Sailor, M. J.; Ghadiri, M. R. Macroporous P-Type Silicon Fabry−Perot Layers. Fabrication, Characterization, and Applications in Biosensing. *J. Am. Chem. Soc.* **1998**, *120*, 12108–12116.

(49) Sweetman, M. J.; Shearer, C. J.; Shapter, J. G.; Voelcker, N. H. Dual Silane Surface Functionalization for the Selective Attachment of Human Neuronal Cells to Porous Silicon. *Langmuir* **2011**, *27* (15), 9497–9503.

(50) Krismastuti, F. S. H.; Brooks, W. L. A.; Sweetman, M. J.; Sumerlin, B. S.; Voelcker, N. H. A Photonic Glucose Biosensor for Chronic Wound Prognostics. *J. Mater. Chem. B* **2014**, *2* (25), 3972–3983.

(51) Aissaoui, N.; Bergaoui, L.; Landoulsi, J.; Lambert, J. F.; Boujday, S. Silane Layers on Silicon Surfaces: Mechanism of Interaction, Stability, and Influence on Protein Adsorption. *Langmuir* **2012**, *28* (1), 656–665.

(52) Futscher, M. H.; Philipp, M.; Müller-Buschbaum, P.; Schulte, A. The Role of Backbone Hydration of Poly(N-Isopropyl Acrylamide) Across the Volume Phase Transition Compared to Its Monomer. *Sci. Rep.* **2017**, *7* (1), 1–10.

(53) Zangooie, S.; Bjorklund, R.; Arwin, H. Water Interaction with Thermally Oxidized Porous Silicon Layers. *J. Electrochem. Soc.* **1997**, *144* (11), 4027–4035.

(54) Jarvis, K. L.; Barnes, T. J.; Prestidge, C. A. Thermal Oxidation for Controlling Protein Interactions with Porous Silicon. *Langmuir* **2010**, *26* (17), 14316–14322.

(55) Plunkett, K. N.; Zhu, X.; Moore, J. S.; Leckband, D. E. PNIPAM Chain Collapse Depends on the Molecular Weight and Grafting Density. *Langmuir* **2006**, *22* (9), 4259–4266.

(56) Arshavsky-Graham, S.; Boyko, E.; Salama, R.; Segal, E. Mass Transfer Limitations of Porous Silicon-Based Biosensors for Protein Detection. *ACS Sens.* **2020**, *5* (10), 3058–3069.

(57) Hill, A. V. The Possible Effects of the Aggregation of the Molecules of Hemoglobin on Its Dissociation Curves. *J. Physiol.* **1910**, *40*, iv–vii.

(58) Kurganov, B. I.; Lobanov, A. V.; Borisov, I. A.; Reshetilov, A. N. Criterion for Hill Equation Validity for Description of Biosensor Calibration Curves. *Anal. Chim. Acta* **2001**, *427* (1), 11–19.

(59) Terracciano, M.; De Stefano, L.; Borbone, N.; Politi, J.; Oliviero, G.; Nici, F.; Casalino, M.; Piccialli, G.; Dardano, P.; Varra, M.; Rea, I. Solid Phase Synthesis of a Thrombin Binding Aptamer on Macroporous Silica for Label Free Optical Quantification of Thrombin. *RSC Adv.* **2016**, *6* (90), 86762–86769.

(60) Urmann, K.; Reich, P.; Walter, J. G.; Beckmann, D.; Segal, E.; Scheper, T. Rapid and Label-Free Detection of Protein a by Aptamer-Tethered Porous Silicon Nanostructures. *J. Biotechnol.* **2017**, *257*, 171–177.

(61) Arshavsky-Graham, S.; Urmann, K.; Salama, R.; Massad-Ivanir, N.; Walter, J. G.; Scheper, T.; Segal, E. Aptamers vs. Antibodies as Capture Probes in Optical Porous Silicon Biosensors. *Analyst* **2020**, *145* (14), 4991–5003.

(62) James N. Weiss. The Hill Equation Revisited: Uses and Misuses. *FASEB J.* **1997**, *11*, 835–841.

(63) Gunther, G. R.; Wang, J. L.; Yahara, I.; Cunningham, B. A.; Edelman, G. M. Concanavalin A Derivatives with Altered Biological Activities. *Proc. Natl. Acad. Sci. U. S. A.* **1973**, *70* (4), 1012–1016.

(64) Garner, B. W.; Cai, T.; Ghosh, S.; Hu, Z.; Neogi, A. Refractive Index Change Due to Volume-Phase Transition in Polyacrylamide Gel Nanospheres for Optoelectronics and Bio-Photonics. *Appl. Phys. Express* **2009**, *2* (5), 32–35.

(65) Ramamurthy, T.; Bhattacharya, S. K.; Uesaka, Y.; Horigome, K.; Paul, M.; Sen, D.; Pal, S. C.; Takeda, T.; Takeda, Y.; Nair, G. B. Evaluation of the Bead Enzyme-Linked Immunosorbent Assay for Detection of Cholera Toxin Directly from Stool Specimens. *J. Clin. Microbiol.* **1992**, *30* (7), 1783–1786.